Chaos and hyperchaos via secondary Neimark–Sacker bifurcation in a model of radiophysical generator

Nataliya Stankevich, Alexander Kuznetsov, Elena Popova & Evgeniy Seleznev

Nonlinear Dynamics
An International Journal of Nonlinear Dynamics and Chaos in Engineering Systems

ISSN 0924-090X
Volume 97
Number 4

Nonlinear Dyn (2019) 97:2355-2370
DOI 10.1007/s11071-019-05132-0

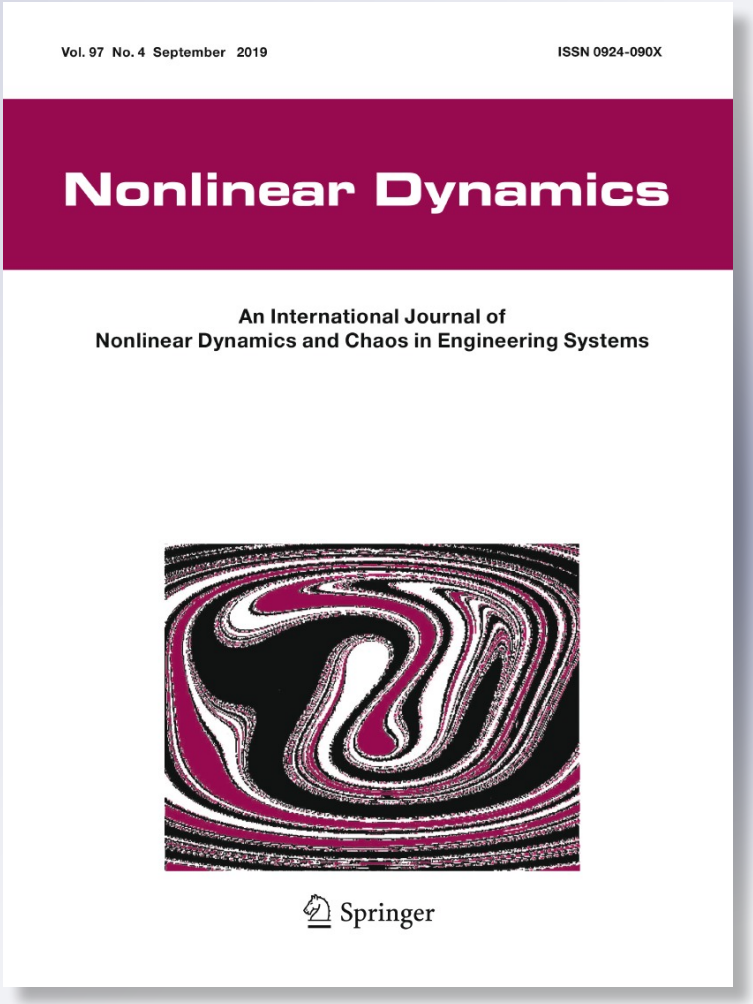

Springer

Nonlinear Dyn (2019) 97:2355–2370
https://doi.org/10.1007/s11071-019-05132-0

ORIGINAL PAPER

Chaos and hyperchaos via secondary Neimark–Sacker bifurcation in a model of radiophysical generator

Nataliya Stankevich · **Alexander Kuznetsov** · **Elena Popova** · **Evgeniy Seleznev**

Received: 21 February 2019 / Accepted: 11 July 2019 / Published online: 25 July 2019

Abstract Using an example of a radiophysical generator model, scenarios for the formation of various chaotic attractors are described, including chaos and hyperchaos. It is shown that as a result of a secondary Neimark–Sacker bifurcation, a hyperchaos with two positive Lyapunov exponents can occur in the system. A comparative analysis of chaotic attractors born as a result of loss of smoothness of an invariant curve, as a result of period-doubling bifurcations, and as a result of secondary Neimark–Sacker bifurcation was carried out.

Keywords Hyperchaos · Secondary Neimark–Sacker bifurcation · Quasiperiodic oscillations · Multistability · Lyapunov exponents

Mathematics Subject Classification 37C55 · 37E45 · 37E99

N. Stankevich (✉)
Department of Radio-Electronics and Telecommunication, Yuri Gagarin State Technical University of Saratov, Saratov, Russia
e-mail: stankevichnv@mail.ru

N. Stankevich · A. Kuznetsov · E. Popova · E. Seleznev
Saratov Branch, Kotel'nikov's Institute of Radio-Engineering and Electronics of RAS, Saratov, Russia

N. Stankevich
Department of Applied Cybernetics, Saint-Petersburg State University, Saint-Petersburg, Russia

1 Introduction

The chaos generated by nonlinear dynamical systems was discovered in the first half of the twentieth century. Chaotic dynamics is a fundamental property of nonlinear systems, which was revealed in nearly all areas of science, namely physics, radiophysics, optics, biophysics, Josephson contact dynamics, neurodynamics, mechanics, chemistry, etc. [1–3]. During that time, numerous studies on the properties of chaos were conducted, the scenarios of chaos emergence were discovered, and multiple applications productively using dynamical chaos were developed.

Chaos is most reliably diagnosed using Lyapunov exponents [4,5]. According to the number of positive Lyapunov exponents, hyperchaos can be classified when there are two or more positive exponents in the spectrum. To this date, the properties of dynamical chaos with one positive Lyapunov exponent are described in detail. Also, a sufficiently large number of models with hyperchaos were presented, among others, in [6–15]. However, the scenarios of hyperchaos formation are poorly studied. One of the scenarios described in [16–23] is associated with riddling bifurcation. The authors described the transition from chaos to hyperchaos in three stages: (i) the saddle-repeller bifurcation of a particular unstable periodic orbit usually of a low period, (ii) the appearance of a repelling node in the saddle-node bifurcation, after which the chaotic attractor becomes riddled, (iii) the absorption of the repeller

originally located beyond the attractor by the growing attractor. Also we would like to mention papers [24–26] where different scenarios of chaos formation were discussed on the example of a three-dimensional map. The scenarios discussed in [24–26] are associated with destruction of torus. In addition, the papers [24,25] demonstrated the possibility of hyperchaos on the parameter plane.

Overall, a review of the models with quasiperiodic behavior shows that in such systems hyperchaos appears quite often with variation of parameters [14,27–30]. For example, in a recent paper [14], a model with hyperchaos was proposed, in which quasiperiodic oscillations were observed as well. It is typical for flows [27–29], as well as maps [24–26]. In a recent paper [27], a possibility of hyperchaos occurring via secondary Neimark–Sacker bifurcation on example of two coupled antiphase-excited Toda oscillators was shown. Also in the systems with stable multi-frequency quasiperiodic oscillations, hyperchaos with several positive Lyapunov exponents is usually observed [31,32].

The main goal of the present paper is to describe formation of the hyperchaos via secondary Neimark–Sacker bifurcation in numerical experiments using the simplest flow model. In our publication, we will analyze the formation of different chaotic attractors including hyperchaos on example of autonomous four-dimensional model with quasiperiodic dynamics. The paper is structured as follows. In Sect. 2, we are going to describe the model in question. In Sect. 3, we will discuss specific features of the parameter plane and localize the domains of existence of various chaotic attractors. In Sect. 4, we will describe in detail and compare the features of different types of chaotic attractors' formation including hyperchaos.

2 Object of study

A minimal dimension of a dynamical flow system in which hyperchaos can occur is four ($N = 4$). In papers [33,34], an autonomous four-dimensional system was proposed. This system represents a radiophysical generator, in which autonomous two-frequency quasiperiodic oscillations were implemented:

$$\begin{aligned}
\dot{x} &= mx + y - x\varphi - dx^3,\\
\dot{y} &= -x,\\
\dot{z} &= \varphi,\\
\dot{\varphi} &= -\gamma\varphi + \gamma\Phi(x) - gz,
\end{aligned} \tag{1}$$

where $\Phi(x) = \frac{1+sgnx}{2}x^2$, $sgnx = \begin{cases} 1, x > 0 \\ -1, x \le 0. \end{cases}$

Here, x, y, z and φ are dynamical variables. The first two equations in system (1) is van der Pol oscillator and the other two describe feedback loops. m is the parameter of excitation, d is the parameter of nonlinear dissipation, γ is the parameter of damping, and g is the inertia parameter. In [33], it was shown that in system (1), a Neimark–Sacker bifurcation produces a two-frequency torus; several bifurcations of the torus doubling, and then torus destruction through the loss of smoothness of an invariant curve, as well as the possible internal synchronization were demonstrated. In [35], it was shown that in system (1) on the base of the synchronization tongue of period-4, a secondary Neimark–Sacker bifurcation occurs. In the present paper, we will consider in detail the parameter plane in the vicinity of secondary Neimark–Sacker bifurcation, investigate the further transformations of the two-frequency torus at variation of parameters and describe the features of formation of chaotic dynamics.

3 Dynamical regimes: chaos and hyperchaos

A convenient tool for studying complex dynamical systems which allows to localize areas of quasiperiodicity, chaos and hyperchaos is the method of charts of Lyapunov exponents [5]. The full spectrum of the Lyapunov exponents was calculated with Benettin algorithm and Gramm–Schmidt orthogonalization [4]. We have to mention, that, strictly speaking, in our numerical experiments, we determined so-called "finite-time local Lyapunov exponents" [36,37]. It means that Lyapunov exponents may vary for different trajectories and their computation were implemented for a finite-time interval. In numerical experiments, we can vary interval between renormalizations in Benettin's scheme changing finite-time interval and accuracy of computation. Increase in accuracy leads to an increase in time of computation, and we should choose trade-off between these characteristics. For construction charts, we use time interval between renormalizations equal to 0.1 and make 70,000 iterations (it corresponds to phase trajectory length 7000); for separate points we check the accuracy and use time interval equal to 10.0. Further,

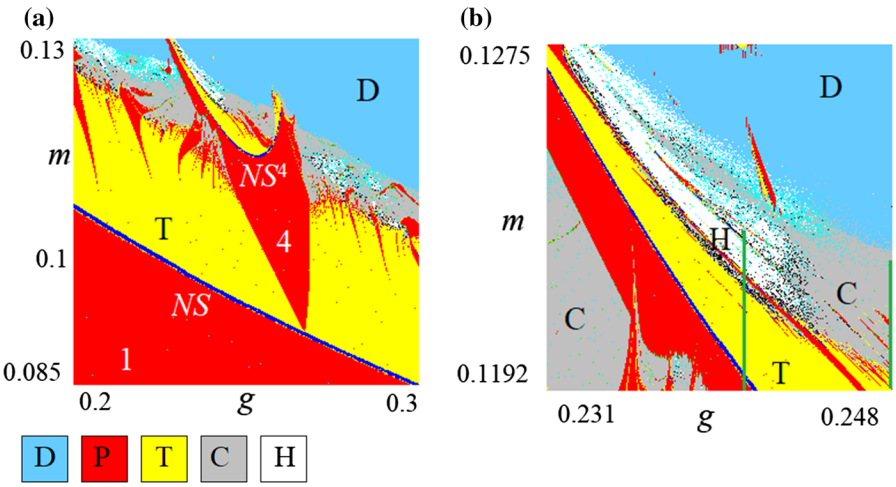

Fig. 1 Chart of Lyapunov exponents for system (1) and it zoomed fragment in the vicinity of transition from two-frequency quasiperiodic torus to chaos. *NS* is Neimark–Sacker bifurcation, NS^4 is secondary Neimark–Sacker bifurcation on the base of the period-4 limit cycle

we will use term "Lyapunov exponents," suggesting "finite-time local Lyapunov exponents."

Figure 1 shows a chart of Lyapunov exponents for model (1) in the vicinity of the period-4 tongue (a) and a zoomed fragment in the vicinity of the torus-chaos transition (b). These charts were constructed as follows: For each point of the parameter plane, the full spectrum of the Lyapunov exponents was calculated. Depending on the spectrum signature, the point on the parameter plane was colored in one or another color in accordance with the palette presented in the bottom of Fig. 1. (Table 1 also shows the signature of the regimes and its symbols.) In Fig. 1a, the numbers 1 and 4 designate the areas of periodic oscillations with the corresponding period, the letters NS and NS^4 note the Neimark–Saker bifurcation lines based on the limit cycles of period-1 and period-4, respectively.

Figure 1 shows that with an increase in the parameter m, the birth of a two-frequency torus is observed on the basis of the limit cycle of period-1. Figure 2a shows two-dimensional projections of the phase portraits in the Poincaré sections by surface $x = 0$ for the limit cycle of period-1 (fixed point) and the torus born on its base (invariant curve). Within the domain of two-frequency quasiperiodicity, synchronization tongues with different winding numbers are observed. The most expressed tongue is the tongue of period-4. Figure 2b shows two-dimensional projections of the phase portraits in the Poincaré sections corresponding to two adjacent values of the parameter m before and after the birth of the limit cycle of period-4 on the torus. The peculiarity of this tongue is that with an increase in the parameter m inside it, a secondary Neimark–Sacker bifurcation (NS^4) occurs, and on the basis of the limit cycle of period-4, a two-frequency torus is born again. For this bifurcation, one can see (Fig. 2c) that in the vicinity of each of the fixed points, an invariant curve is born, i.e., the torus becomes a 4-turn, it is so-called multilayered torus [38,39]. Along secondary Neimark–Sacker bifurcation line, Arnold tongues are observed; however, in this case, the synchronization will occur on the base of multilayered torus. Thus, we will see hierarchy of synchrony regimes corresponding to different multilayered tori.

Table 1 Accordance between signature of the Lyapunov exponents spectrum of observed regimes and symbols used for the charts of Lyapunov exponents

Regime	Symbol	Spectrum of Lyapunov exponents
Periodic	P	$\Lambda_1 = 0, \Lambda_4 < \Lambda_3 < \Lambda_2 < 0$
Quasiperiodic	T	$\Lambda_1 = 0, \Lambda_2 = 0, \Lambda_4 < \Lambda_3 < 0$
Chaos	C	$\Lambda_1 > 0, \Lambda_2 = 0, \Lambda_4 < \Lambda_3 < 0$
Hyperchaos	H	$\Lambda_2 > \Lambda_1 > 0, \Lambda_3 = 0, \Lambda_4 < 0$
Divergency	D	

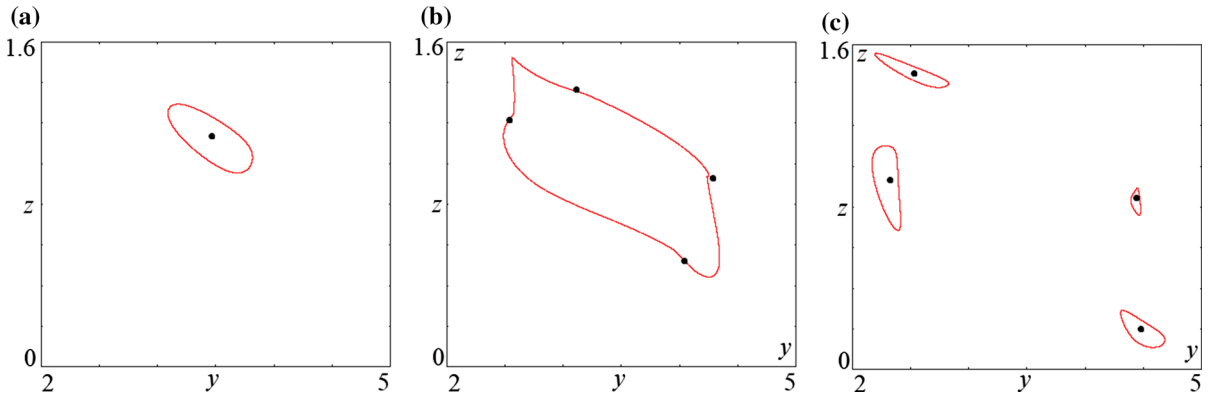

Fig. 2 Two-dimensional projections of phase portraits in the Poincaré section by surface $x = 0$ demonstrating main bifurcations in system (1) at $g = 0.25$: **a** Neimark–Sacker bifurcation, $m = 0.095$ (black dot corresponding to the limit cycle P1), $m = 0.097$ (red invariant curve corresponding to the torus T1:P1); **b** synchronization on the torus, $m = 0.106$ (red invariant curve corresponding to the torus T1:P1), $m = 0.107$ (black dots corresponding to the limit cycle P4:T1:P1); **c** secondary Neimark–Sacker bifurcation, $m = 0.115$ (black dots corresponding to the limit cycle P4:T1:P1), $m = 0.116$ (red invariant curves corresponding to the torus T4:P4:T1:P1). (Color figure online)

With a further increase in the parameter m, the torus collapses with the formation of chaotic attractor. At the same time, as seen on the parameter plane, it is formed as chaos with one positive Lyapunov exponent (gray color), as well as hyperchaos with two positive Lyapunov exponents (white color). Figure 1b shows a zoomed fragment of the parameter plane, where the transition to chaotic and hyperchaotic dynamics is shown in more detail.

To discuss and trace the dynamics of the system, let us introduce two indicators: the cycle number and the torus number, with which one can monitor the origin of the limit cycle or torus, as well as its position in the hierarchy. These indicators will include sequences of numbers corresponding to periods of a limit cycle and tori, with an additional letter designation indicating the type of dynamical behavior T or P for a torus or a limit cycle, respectively. So, for instance, the basic limit cycle will have the cycle number P1; after the Neimark–Sacker bifurcation occurred to it, a torus appeared with the torus number T1:P1, which means that the torus originated on the basis of the limit cycle of period-1. The limit cycle of period-4 appeared on torus T1:P1 will have the cycle number P4:T1:P1, and the torus resulting from the secondary Neimark–Sacker bifurcation on the basis of this cycle will have the torus number T4:P4:T1:P1. When a resonance with period n occurs on the torus T4:P4:T1:P1, we will observe a limit cycle with the cycle number Pn:T4:P4:T1:P1. By the cycle number, we can determine the period of the limit cycle by multiplying all the values near the indicator P, i.e., for the limit cycle with the cycle number Pn:T4:P4:T1:P1, the period of oscillations is equal to $n * 4 * 1$. Using these indicators, we will be able to monitor the place of each cycle and torus in the hierarchy of synchronous cycles and to see its evaluations at varying parameters.

4 Chaos and hyperchaos in the model

Let us investigate in detail the formation of different chaotic attractors. With this purpose, we consider the dynamics of system (1) in dependence on the parameter m for two different fixed values of parameter g: (i) when torus transforms to hyperchaos $g = 0.2407$; (ii) when torus transforms to chaos with one positive Lyapunov exponent, $g = 0.248$. In Fig. 1, two green lines corresponding to these values of parameter g are depicted.

4.1 Formation of hyperchaos via secondary Neimark-Sacker bifurcation

Firstly, let us consider the scenario of the formation of hyperchaos. Figure 3 shows the dependencies of the

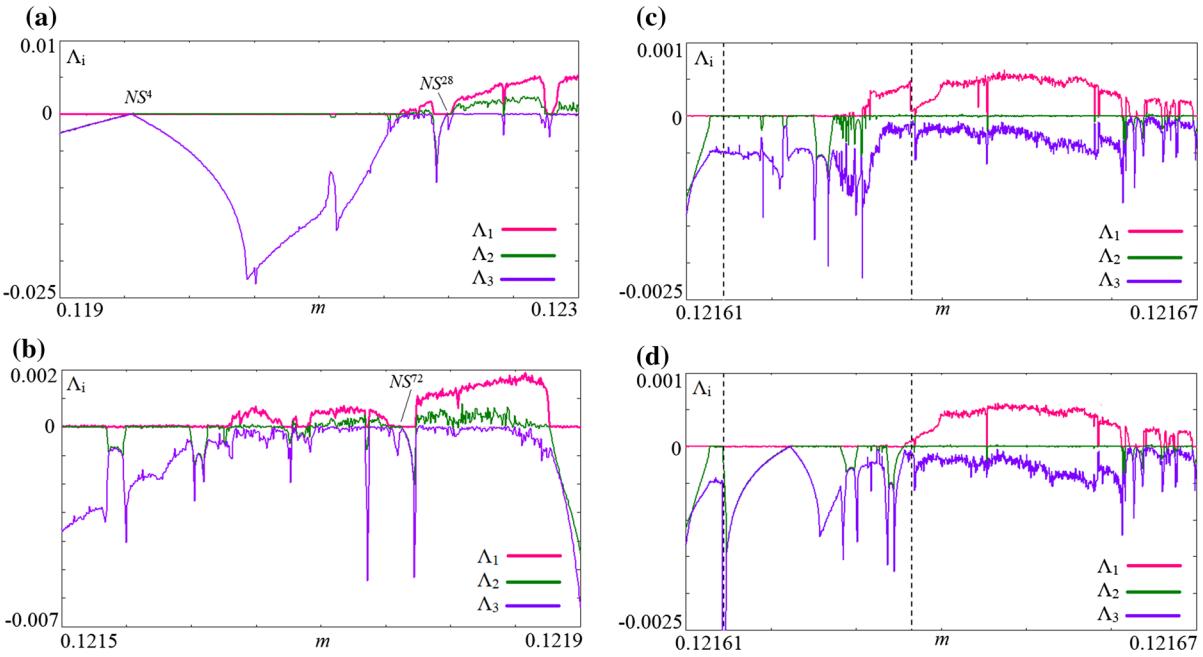

Fig. 3 Dependence of the largest three Lyapunov exponents on the parameter m at $g = 0.2407$ **a** and its zoomed fragments: **b** domain of formation of chaotic dynamics; **c**, **d** domain of multistability

three largest Lyapunov exponents[1] on the parameter m and their zoomed fragments. As shown in Fig. 3a, for $m = 0.119$, the largest exponent equals zero, and the second and third are negative and equal to each other. In the phase space, the limit cycle of period-4 corresponds to this regime. At $m \approx 0.1196$, the two largest Lyapunov exponents become equal to zero and the secondary Neimark–Sacker bifurcation (NS^4) occurs, as a result of which a multilayered two-frequency torus is born.[2] The born 4-turn torus remains stable over a sufficiently large interval of the parameter m. Further, there is an interval of the parameter m, where the second Lyapunov exponent becomes negative, which corresponds to synchronization on the torus. Next, the destruction of the torus with formation of chaos at $m \approx 0.12163$ is observed. For $m > 0.12163$, several domains of chaos can be distinguished, which are separated by a domains of periodic oscillations. In Fig. 3b, a zoomed fragment corresponding to the first domain of chaos is presented. In Fig. 3b, it is clear that chaos is firstly born with one positive Lyapunov exponent. Let us consider in more detail the features of the formation of a chaotic attractor in this domain.

Multistability is observed in the vicinity of the critical point of chaos. Figure 3c, d shows zoomed fragments of the plots of the three largest Lyapunov exponents, constructed with continuation method of changing of initial conditions[3] for different starting initial conditions. When $m = 0.12162$ in Fig. 3c, the initial conditions were fixed as $(0, 2.1391, 1.2333, -1.3559)$, the system (1) quasiperiodic dynamics demonstrated; and for Fig. 3d, initial conditions were fixed as $(0, -4.5742, 0.9503, -1.1037)$; then, in system (1), periodic dynamics is revealed. Thus, in Fig. 3c, plots are focused on the visualization of the transformations of the base invariant curve, and in Fig. 3d, plots visualize the changing of coexisting attractor.

[1] System (1) is four-dimensional and in fact it has four Lyapunov exponents, but the fourth exponent is always negative, and we did not add it to the plots.

[2] In accordance with [40,41], if for a flow dynamical system at variation of the parameter, the largest Lyapunov exponent is equal zero and two of the following are negative and equal to each other before bifurcation, and if two of the largest Lyapunov exponents are equal zero and the third is negative after bifurcation, it indicates the Neimark–Sacker bifurcation.

[3] Also sometimes it is called adiabatic initial conditions, i.e., for each new value of the parameter, the initial conditions were chosen as the final state attained for the previous value of the parameter.

As shown in Fig. 3c, when $m \approx 0.121612$, a new limit cycle (periodic regime) appears, which with further increase in the parameter m coexists with the main 4-turn torus. Multistability between these attractors and attractors resulting from their transformations are observed up to $m \approx 0.121642$. Dashed lines in Fig. 3c, d mark domain of multistability in the parameter space. In Fig. 3c, it is clearly seen that as the parameter m increases, resonant cycles appear on the surface of the two-frequency torus; it correspond to dips of the second Lyapunov exponent in the negative region, and then the 4-turn invariant torus undergoes destruction and a chaotic attractor is formed on it base. In Fig. 3d, one can see that the coexisting limit cycle at $m \approx 0.121621$ undergoes the secondary Neimark–Sacker bifurcation; we see that two nonzero Lyapunov exponents (Λ_2 and Λ_3) are equal to each other before bifurcation. With further increase in the parameter m, resonances on the torus (dips in the negative region of the second Lyapunov exponent Λ_2 are visible) and torus destruction are also observed with the formation of chaos. Bifurcations of coexisting attractors occur independently of each other.

The values of the Lyapunov exponents for coexisting attractors are close to each other, which makes it difficult to analyze them. Let us consider what happens in the phase space when the parameter m is varied in the same way as in Fig. 3c, d.

Figure 4 presents two-dimensional projections of phase portraits in the Poincaré section by a surface $x = 0$ for model (1). The figures show the vicinity of the one of four invariant curves of the 4-turn torus with torus number T4:P4:T1:P1 (left column), as well as its enlarged fragment, visualizing the structure of attractors (right column). The structure of the phase space in the vicinity of the other three invariant curves is similar. The coexisting attractors are shown by red and blue dots; red attractors correspond to the plot of Lyapunov exponents shown in Fig. 3c, blue to 3d. The considered transformations occur with small variations of the parameter; in the presented examples, the parameter m changes with accuracy about 10^{-5}, which imposes certain requirements on the accuracy of calculations. For the above example of attractor, the full spectrum of Lyapunov exponents was calculated with high accuracy, and their values are presented in Table 2.

Figure 4a shows an invariant curve with torus number T4:P4:T1:P1 that has a rather complex form; however, in the zoomed fragment (right column), it can be seen that the invariant curve is smooth and continuous. In Table 2, one can see that the spectrum of Lyapunov exponents of the attractor shown in Fig. 4a contains two zero exponents, which corresponds to the two-frequency quasiperiodic regime.

When $m \approx 0.121612$ in the system, the limit cycle of period-72 is born, which coexists with the invariant curve. In the Poincaré section, 72 fixed points correspond to this limit cycle (blue dots in Fig. 4a), one zero and three negative Lyapunov exponents correspond to this regime (Table 2). The limit cycle is born very close to the torus; however, the torus does not disappear, and they coexist in a sufficiently large interval of the parameter m. Such kind of multistability is observed in many systems [43,44] and is usually associated with symmetries in the system. The structure of the limit cycle of period-72 in the Poincaré section corresponds to the invariant curve of the torus with torus number T4:P4:T1:P1; in the neighborhood of each of the four invariant curves, 18 fixed points appear. The limit cycle of period-72 has the cycle number P18:T4:P4:T1:P1.

With a further increase in the parameter m, changes with coexisting attractors occur. So on the basis of invariant curve, higher-order resonances appear (red dots in Fig. 4b). A resonant cycle of period-448 is born on the surface of the torus, 112 fixed points appear on each invariant curve (Fig. 4b), and the cycle number is P112:T4:P4:T1:P1. Further the invariant curve becomes more complex, sharp angles appear, and at $m \approx 121631$, the invariant curve is transformed into a chaotic attractor (Fig. 4c–e); in accordance with [25], we observe torus-chaos. For chaotic attractors, the largest Lyapunov exponent becomes positive, and the second is zero (Table 2). In this case, there is a blowing of invariant curve. Thus, as a result of this scenario, chaos is born with one positive and one zero Lyapunov exponents.

The coexisting limit cycle of period-72 with the cycle number P18:T4:P4:T1:P1 is also changed with the increase in the parameter m (blue attractors). When $m \approx 0.121621$, a secondary Neimark–Sacker bifurcation takes place resulting in a 72-turn torus with the torus number T18:P18:T4:P4:T1:P1 to which 72 invariant curves correspond in the Poincaré section (Fig. 4b). An additional zero exponent appears in the spectrum of Lyapunov exponents (Table 2). With further increase in the parameter m, resonances are also observed for this attractor. In this case, period of the limit cycles and the cycle number increases. For example, one can

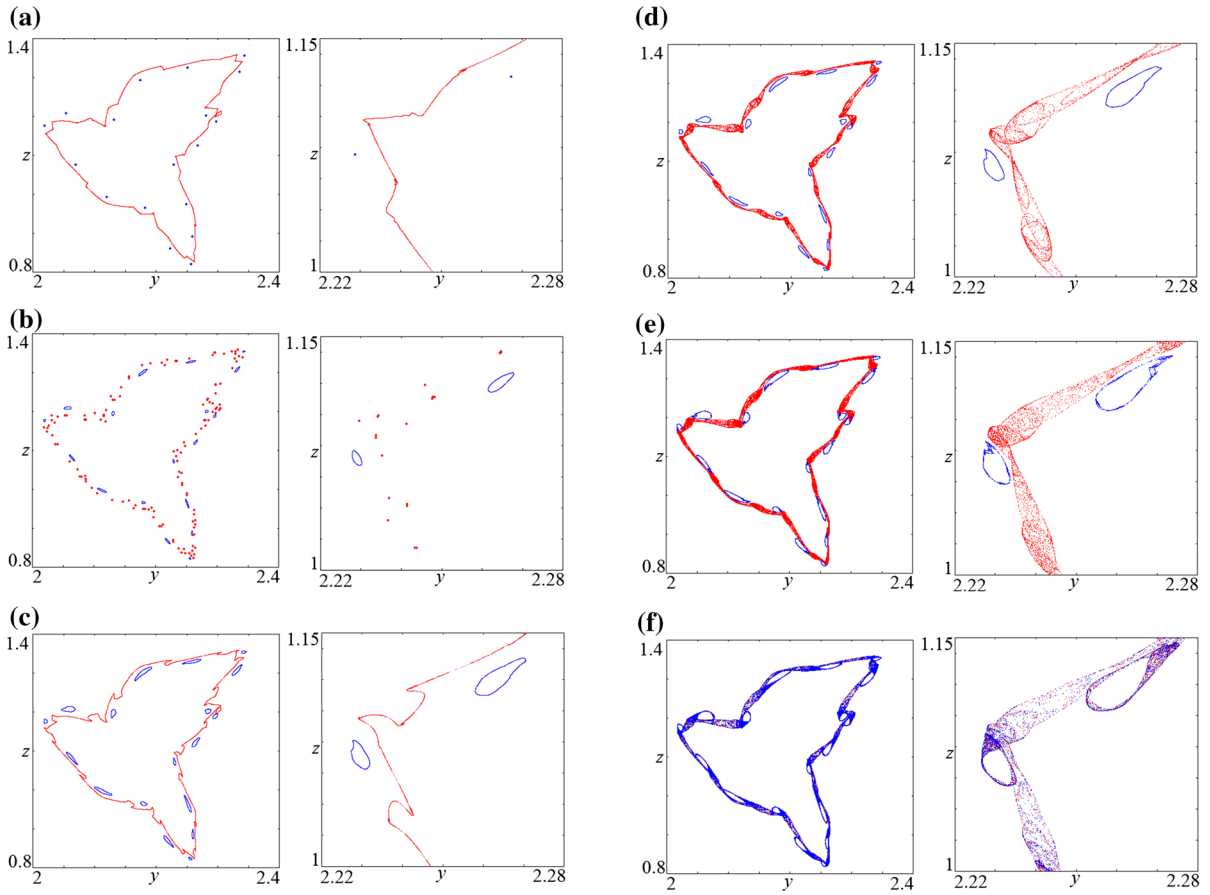

Fig. 4 Two-dimensional projections of phase portraits in the Poincaré section by surface $x = 0$ demonstrating multistability and transition to chaos with one positive Lyapunov exponent, $g = 0.2407$; **a** $m = 0.121615$, T4:P4T1:P1 (red) and P18:T4:P4:T1:P1 (blue); **b** $m = 0.121625$, P112:T4:P4T1:P1 (red) and T18:P18:T4:P4:T1:P1 (blue); **c** $m = 0.121631$, chaos (red) and T18:P18:T4:P4:T1:P1 (blue); **d** $m = 0.121632$, chaos (red) and T18:P18:T4:P4:T1:P1 (blue); **e** $m = 0.121636$, chaos (red) and chaos (blue); **f** $m = 0.121640$, merged chaos. (Color figure online)

Table 2 Signature of the spectrum of the Lyapunov exponents for attractors at transition to chaos, $g = 0.2407$

m	Regime	Λ_1	Λ_2	Λ_3	Λ_4
0.121615	T^4	0.0000	0.0000	−0.0005	−0.0883
0.121615	P^{72}	0.0000	−0.0012	−0.0013	−0.0863
0.121625	P^{448}	0.0000	−0.0001	−0.0012	−0.0875
0.121625	T^{72}	0.0000	0.0000	−0.0006	−0.0882
0.121631	C	0.0001	0.0000	−0.0010	−0.0879
0.121631	T^{72}	0.0000	0.0000	−0.0003	−0.0885
0.121632	C	0.0003	0.0000	−0.0004	−0.0887
0.121632	T^{72}	0.0000	0.0000	−0.0002	−0.0886
0.121636	C	0.0004	0.0000	−0.0002	−0.0890
0.121636	C	0.0001	0.0000	−0.0001	−0.0887
0.121640	C	0.0004	0.0000	−0.0002	−0.0890

observe the limit cycle of period-360 with the cycle number P5:T18:P18:T4:P4:T1:P1. Then, the 72-turn torus is destroyed and a chaotic attractor is formed. Figure 4d presents example of coexisting chaotic attractors. Attractors have a different structure, in accordance with the invariant curves, on the basis of which they appeared; for the first case, four destroyed invariant curves are observed, and for the second case, 72 destroyed invariant curves are observed. For both cases, it is clearly seen that the strange chaotic attractor in the Poincaré section is localized in the vicinity of the base invariant curve, and no filling of the invariant curve inside is observed.

Remark that the largest Lyapunov exponents for coexisting attractors are positive; however, the absolute value of the exponents is different (Table 2). For attractor born as a result of the destruction of a 4-turn invariant curve, the largest Lyapunov exponent is four times greater than for a chaotic attractor born on the basis of a 72-turn torus, and for both cases, the order of values is 10^{-4}.

With further increase in the parameter m at $m \approx 0.12164$, two chaotic attractors merge and form a single complex attractor. The basis of the structure of the new chaotic attractor is the 4-turn torus (T4:P4:T1:P1), but the loops of the 72-turn torus (T18:P18:T4:P4:T1:P1) are embedded in to chaotic attractor. The largest Lyapunov exponent corresponds to a more developed chaotic regime, i.e., chaos based on a 4-turn invariant curve (Table 2).

The plots of Lyapunov exponents (Fig. 3) and Table 2 clearly show that the largest Lyapunov (positive) exponent for chaotic attractor born as a result of the destruction of 4-turn torus is greater than the largest exponent for chaos born as a result of destruction of 72-turn torus. In the plots of Lyapunov exponents with a further increase in the parameter m in a certain interval of parameter ($m < 0.121657$), the largest exponent of the merged attractor remains at the same level, and for $m > 0.121657$, its value begins to decrease. Figure 5 presents fragments of two-dimensional projection of the phase portraits in the Poincaré section, where the transformations of attractors are shown with the corresponding variation of the parameter m and decrease in the largest Lyapunov exponent. The attractor is a merging of two chaotic attractors up to $m \approx 0.12657$, and it preserves the structure of 4-turn torus (Fig. 5a). At $m = 0.121657$, the phase points condense in the vicinity of the invariant curves of 72-turn torus (Fig. 5b). Further, there are resonances on the torus. Figure 5c shows an example of the limit cycle with the cycle number P21:T18:P18:T4:P4:T1:P1 and, respectively, a period equal 1512. Figure 5d shows the limit cycle with the cycle number P5:T18:P18:T4:P4:T1:P1 and, accordingly, period-360. At $m \approx 0.121678$, hyperchaos formation is observed. Figure 5e shows an example of hyperchaotic attractor at $m = 0.12168$; Lyapunov exponents take the following values: $\Lambda_1 = 0.0003$, $\Lambda_2 = 0.0001$, $\Lambda_3 = 0$, $\Lambda_4 = -0.0891$. In this case, fulfilling of the invariant curve inside happens when a hyperchaos occurs. The hyperchaotic attractor in the Poincaré section has form of 72 chaotic "islands."

With a further increase in the parameter m, periodicity windows are observed, in which the secondary

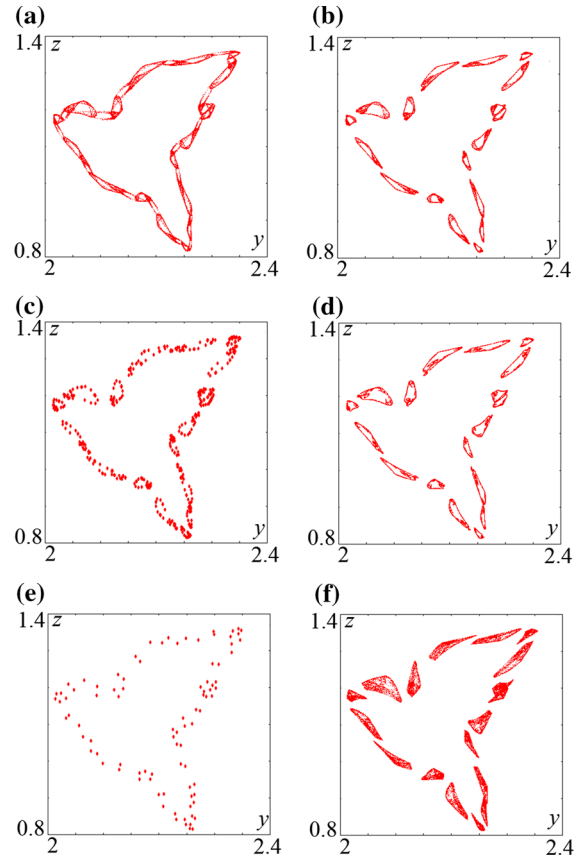

Fig. 5 Two-dimensional projections of phase portraits in the Poincaré section by surface $x = 0$ demonstrating formation of hyperchaos, $g = 0.2407$; **a** $m = 0.121656$, chaos; **b** $m = 0.121657$, chaos; **c** $m = 0.121658$, P21:T18:P18:T4:P4:T1:P1; **d** $m = 0.12166$, chaos; **e** $m = 0.121675$, P5:T18:P18:T4:P4:T1:P1, **f**) $m = 0.12168$, hyperchaos

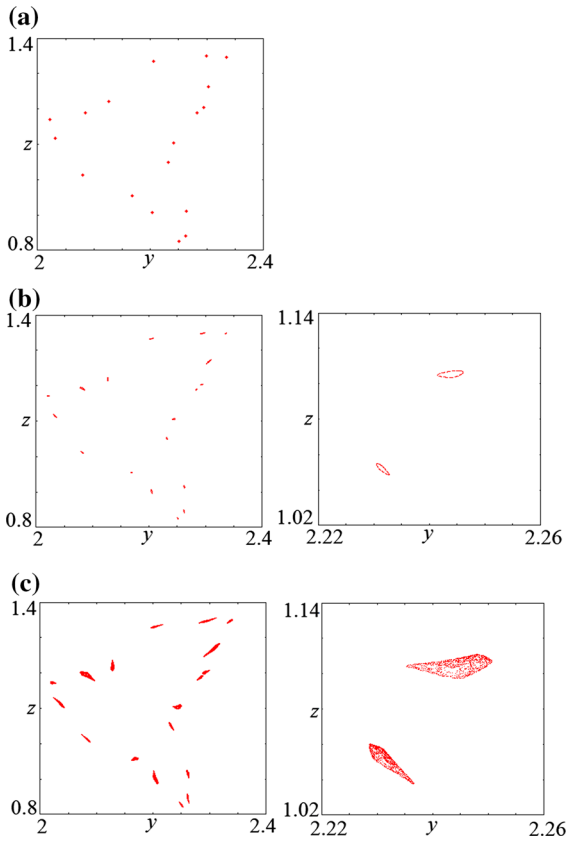

Fig. 6 Two-dimensional projections of phase portraits in the Poincare section by surface $x = 0$ demonstrating transition to hyperchaos via secondary Neimark–Sacker bifurcation on the base limit cycle of period-72, $g = 0.2407$; **a** $m = 0.12177$, P18:T4:P4:T1:P1; **b** $m = 0.12176$, T18:P18:T4:P4:T1:P1; **c** $m = 0.12205$, hyperchaos

Neimark–Sacker bifurcation occurs again, after which the hyperchaos forms. On fragments of plots of Lyapunov exponents, the corresponding transformations are clearly visible on the basis of the limit cycles of period-72 (Fig. 3a) and period-28 (Fig. 3b), denoted by the symbols NS^{72} and NS^{28}. Consider in more detail the features of the formation of hyperchaos for these windows.

Let us now turn to Fig.3b, in which the letter NS^{72} denotes the secondary Neimark–Sacker bifurcation at $m \approx 0.121765$. In this case, the secondary Neimark–Sacker bifurcation occurs with a decrease in the parameter m, which is also indicated by the equality of two nonzero Lyapunov exponents (Λ_2 and Λ_3) before the bifurcation. For this parameter area, multistability is not observed. The secondary Neimark–Sacker bifurcation occurs on the basis of the limit cycle of period-72 with the cycle number P18:T4:P4:T1:P1; as a result, a two-frequency quasiperiodic regime appears, which is represented in phase space by the 72-turn torus with a torus number T18:P18:T4:P4:T1:P1. Figure 6a shows two-dimensional projection of the phase portrait in the Poincaré section by the surface $x = 0$ at $m = 0.12177$, which corresponds to the limit cycle of period-72. The figure clearly shows a set of discrete points. The structure of the phase space corresponding to the limit cycle of period-4, on the basis of which such dynamics is developed, has also been preserved. On each of the four invariant curves, 18 fixed points appeared. When the parameter m decreases, the Neimark–Sacker bifurcation occurs on the basis of the limit cycle of period-72, as a result of which the two-frequency multilayered torus (T18:P18:T4:P4:T1:P1) is born again. The corresponding transformation is illustrated in Fig. 6b ($m = 0.12176$). In the vicinity of each fixed point, a smooth closed invariant curve is born, with the general structure of the phase space, characteristic of the limit cycle with cycle number P4:T1:P1, also preserved. With further increase in the parameter m, the torus collapses and a hyperchaos with two positive Lyapunov exponents is formed; an example of the phase portrait is shown in Fig. 6c ($m = 0.12175$). The phase space inside the invariant curves is filled in and the "islands" of chaotic dynamics are formed in the Poincaré section. The formation of "islands" of chaos occurs in the following way: the filling occurs inside invariant curves corresponding to the limit cycle of period-72, thus forming four islands of chaotic dynamics, each of which contains 18 more small-scale "islands" of chaos.

Table 3 Signature of the spectrum of the Lyapunov exponents for attractors at transition to hyperchaos via secondary Neimark–Sacker bifurcation on the base of limit cycle of period-72, $g = 0.2407$

m	Regime	Λ_1	Λ_2	Λ_3	Λ_4
0.12177	P^{72}	0.0000	−0.0010	−0.0011	−0.0866
0.12176	T	0.0000	0.0000	−0.0004	−0.0882
0.12175	HC	0.0002	0.0001	0.0000	−0.0890

Table 3 also shows the values of Lyapunov exponents for characteristic regimes and attractors presented in Fig.6. As given in Table 4 for the shown chaotic attractors, the values of positive Lyapunov exponents

are of the same order (10^{-4}), as it was in the previous case.

Thus, using the example of the limit cycle of period-72 with the cycle number P18:T4:P4:T1:P1, we observed the formation of a hyperchaos. The domains of parameters with hyperchaos and chaos alternate with each other, but there is a correspondence between the observed chaotic regimes and the configuration of the attractor in the Poincaré section; formation of hyperchaos is associated with the filling of invariant curves inside.

Similar transformations of phase portraits can be observed for the limit cycle of period-28, but for greater values of the parameter m. Let us consider windows of periodicity of the limit cycle of period-28. Synchronization tongue of period-28 is rather pronounced and denoted by the symbol NS^{28} in Fig. 3a. Inside this tongue, the limit cycle of period-28 is observed. A zoomed fragment of graphs of Lyapunov exponents in its vicinity is presented in Fig. 7a. Figure 7a clearly shows that at $m \approx 0.12199$, a secondary Neimark–Sacker bifurcation occurs as a result of which a torus is born, and then a hyperchaos is formed. Figure 7b–d shows the characteristic phase portraits in the Poincaré section; Fig. 7b are the fragments of phase space in the vicinity of one of the invariant curves; Fig. 7d, e shows fully phase space (left column) and zoomed fragment (right column). The structure of the phase space preserves the basic limit cycle of period-4; seven fixed points arise on each invariant curve, which generally corresponds to the limit cycle of period-28 with cycle number P7:T4:P4:T1:P1 (Fig. 7b). With an increase in the parameter m, the secondary Neimark–Sacker bifurcation occurs on the basis of the limit cycle of period-28, and 28 invariant curves corresponding to multilayered torus with torus number T7:P7:T4:P4:T1:P1 are formed in the Poincaré section (Fig. 7c). As a result of the destruction of the 28-turn torus, a hyperchaos is formed. In this case, the phase points fill invariant curve inside. The structure of the phase space is preserved in the form of four "islands" of chaotic dynamics corresponding to limit cycle of period-4, on the basis of which the described hyperchaos is developed. As well as for the limit cycle of period-72, the phase space inside the invariant curves is filled in. Firstly, invariant curves of the 28-turn torus are filled in (Fig. 7d), and then 4-turn invariant curves are also filled in (Fig. 7e), thus forming four islands of chaotic dynamics.

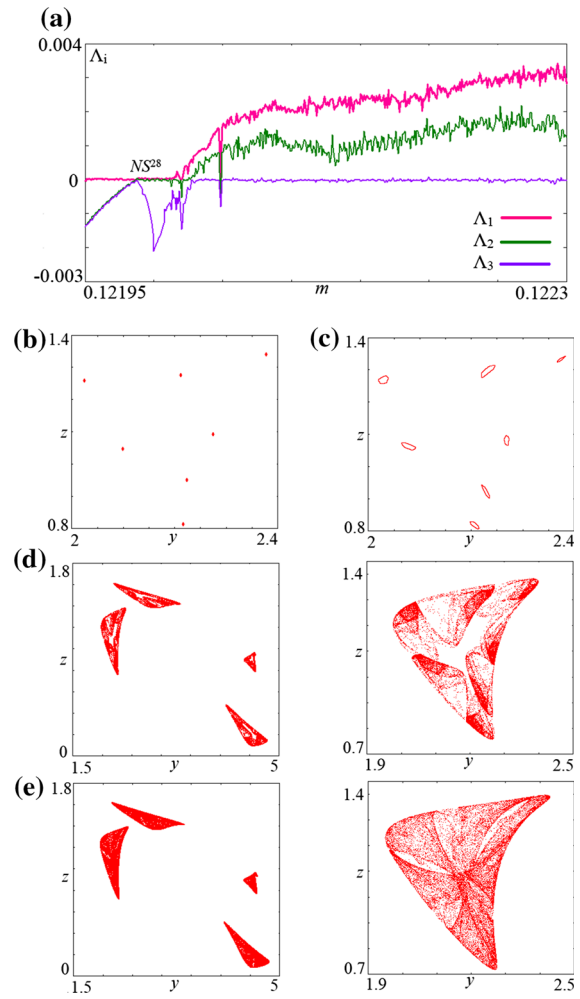

Fig. 7 Dependence of the largest three Lyapunov exponents on the parameter m in the transition to hyperchaos via secondary Neimark–Sacker bifurcation on the base limit cycle of period-28 at $g = 0.2407$, **a** Two-dimensional projections of phase portraits in the Poincaré section by surface $x = 0$ demonstrating transition to hyperchaos via secondary Neimark–Sacker bifurcation on the base limit cycle of period-28, $g = 0.2407$; **b** $m = 0.1219$, P7:T4:P4:T1:P1; **c** $m = 0.122$, T7:P7:T4:P4:T1:P1; **d** $m = 0.12205$, hyperchaos; **e** $m = 0.1223$, hyperchaos

Table 4 presents the values of Lyapunov exponents for attractors shown in Fig. 7, which is fully consistent with the observed regimes. With an increase in the parameter m, an increase in the values of the Lyapunov exponents is observed. If we compare the values of the positive Lyapunov exponents, it is clearly seen that the hyperchaos resulting from the destruction of a torus with a torus number of T7:P7:T4:P4:T1:P1 is characterized by a much larger value.

Table 4 Signature of the spectrum of the Lyapunov exponents for attractors at transition to hyperchaos via secondary Neimark–Sacker bifurcation on the base of limit cycle of period-28, $g = 0.2407$

m	Regime	Λ_1	Λ_2	Λ_3	Λ_4
0.1219	P^{28}	0.0000	−0.0044	−0.0062	−0.0779
0.122	T	0.0000	0.0000	−0.0021	−0.0863
0.12205	HC	0.0016	0.0008	0.0000	−0.0907
0.1223	HC	0.0031	0.0014	0.0000	−0.0925

Thus, in this parameter domain, the formation of chaotic dynamics as a result of the destruction of an invariant curve is observed. As a result of torus destruction, a chaotic attractor with one positive Lyapunov exponent is formed. Also in the system, there is a hierarchy of multilayered tori, the destruction of which leads to the formation of hyperchaos. Fundamental to the emergence of hyperchaos is filling an invariant curve.

4.2 Formation of chaos with one positive Lyapunov exponents

Via the secondary Neimark–Sacker bifurcation, the transition to chaos with one positive Lyapunov exponent is also possible. Within the framework of model (1), such transition can be observed for the same tongue of the limit cycle of the period-4 with cycle number P4:T1:P1, but for large values of the parameter g. Let us consider in more detail the formation of chaos at $g = 0.248$.

In Fig. 8a, plots of the Lyapunov exponents versus the parameter m are presented for $g = 0.248$. As in the previous case for small values of the parameter m, the two-frequency quasiperiodicity is observed. Inside the region of quasiperiodic oscillations, high-order resonances are observed, which correspond to the negative values of the second Lyapunov exponent Λ_2 in Fig. 8a. Figure 9 presents two-dimensional projections of phase portraits in the Poincaré section by a surface $x = 0$. Figure 9a–c demonstrates the transformation of invariant curves during the initial formation of chaos. Figure 9a shows the invariant curves corresponding to 4-turn torus with torus number T4:P4:T1:P1. In this case, the invariant curves are closed, have a simple form, with slight bends. Figure 9b presents the phase portrait for the limit cycle of the period-188 that has arisen on the surface of 4-turn torus. On each of the four invariant curves, 47 fixed points arise; thus, the cycle number for this attractor is P47:T4:P4:T1:P1. After resonance, the invariant curves presented in Fig. 9c have become more complex, but according to the values of the Lyapunov exponents, the regime is still quasiperiodic. Thus, as the parameter m is increased, the complexity of the invariant curve is observed. Then, at $m \approx 0.119587$, a limit cycle occurs on the surface of the 4-turn torus with the cycle number P10:T4:P4:T1:P1 (in Fig. 8a, this cycle is designated by symbol P^{40}), the loss of stability which leads to the appearance of a chaotic attractor.

In the vicinity of the chaos-forming region for $g = 0.248$, as well as for the previous case (Sect. 4.1), multistability is observed. Figure 8c, d shows the plots of Lyapunov exponents constructed for different starting initial conditions at $m = 0.11963$. For Fig. 8c, the starting initial conditions were chosen as $(0, 1.9356, 1.2147, -1.3150)$ and for Fig. 8d, as $(0, 4.6534, 0.1521, -1.3231)$. Multistability is observed in the range of the parameter $m\,(0.119622 - 0.119665)$; this interval is marked by dotted lines in the plots of Lyapunov exponents. As shown in Fig. 8c, a stable limit cycle is observed for this region. When $m \approx 0.119662$, a period-doubling bifurcation occurs, and then the regime is hardly switched to chaotic dynamics.

When $m \approx 0.119622$, a coexisting cycle appears, the dynamics of which can be traced in Fig.8e; the coexisting cycle undergoes a cascade of period-doubling bifurcations with a transition to chaos. Figure 9d–f shows two-dimensional projections of phase portraits in the Poincaré section of coexisting attractors. As shown in Fig. 9d near the limit cycle with the cycle number P10:T4:P4:T1:P1, the limit cycle appears with the same cycle number. With the coexisting cycle, a cascade of period-doubling bifurcations occurs and a chaotic attractor is formed. Figure 9e presents an example of the coexisting limit cycle of period-40 and the chaotic attractor, which arose on the basis of the coexisting cycle. The chaotic attractor is very compressed in phase space and is located near the coexisting limit cycle. The plots of Lyapunov exponents show that as the parameter m is increased, several intervals are observed with the chaotic dynamics of the coexisting attractor, alternating with the periodic one. When approaching the edge of the multistability region, the coexisting attractor becomes periodic. Figure 9f shows an example of a coexisting chaotic attractor, arising from the main limit cycle, and the limit cycle of period-160 (cycle

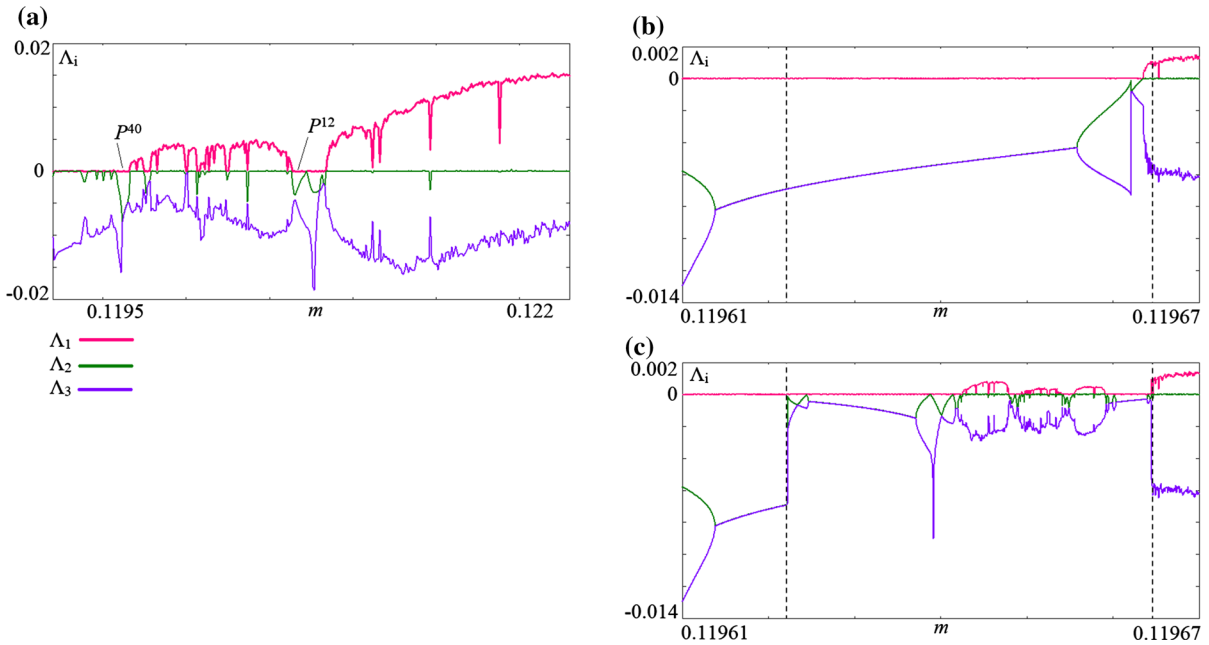

Fig. 8 Dependence of the largest three Lyapunov exponents on the parameter m at $g = 0.248$ **a** and its zoomed fragments: **b**, **c** domain of multistability

number P40:T4:P4:T1:P1). At $m \approx 0.119665$, as well as for the main coexisting attractor, a hard transition to chaos is observed. Such a transition is associated with a crisis of the attractor born as a result of period-doubling bifurcations. The chaotic attractor has a complex structure. However, the form of four invariant curves is preserved. Invariant curves become more rugged and lose smoothness.

For large values of the parameter m inside the periodicity windows, the formation of chaos is observed through a sequence of period-doubling bifurcations. This scenario can be observed for the limit cycle of period-12 with the cycle number P3:T4:P4:T1:P1. (This regime is denoted by symbol P^{12} in Fig. 8a.)

Figure 10 shows the projections of the phase portrait in the Poincaré section by a surface $x = 0$, demonstrating the transformation of the limit cycle of period-12 into a chaotic attractor. Figure 10a–c shows three period-doubling bifurcations. As we can see, the base cycle with cycle number P3:T4:P4:T1:P1 persists the structure of the torus T4:P4:T1:P1. In Fig. 10d, e, two characteristic chaotic attractors are presented. In Table 5, values of the full spectrum of Lyapunov exponents for these chaotic attractors are shown. For the chaotic attractor in Fig. 10d, the largest Lyapunov exponent equals $\Lambda_1 \approx 0.0023$. In this case, the chaotic attractor in the Poincaré section consists of 12 discrete lines, each of which arose with doubling of the limit cycle of period-12. The chaotic attractor has similar structure to the chaotic attractor resulting from the limit cycle of period-40 with the cycle number P10:T4:P4:T1:P1 (Fig. 9e); it is compressed in the phase space. With an increase in the parameter m, chaos becomes more developed, and the attractor again takes the form of the 4-turn torus. In Fig. 10e, four destroyed invariant curves are clearly visible, with characteristic sharp angles near three fixed points that correspond to the resonant cycle, on the basis of which the attractor appeared. For the developed chaos, the largest Lyapunov exponent is equal to $\Lambda_1 \approx 0.0064$. The principal difference between such a chaotic attractor is that in this case, the structure of the phase space characteristic for the tori is persist, but we did not observe formation of chaotic islands (filling invariant curves inside) that are typical for the hyperchaos.

Note that a typical classic Feigenbaum scenario dependence of Lyapunov exponents is observed. The first Λ_1 and the third Λ_3 exponents behave symmetrically with respect to the second Λ_2 (zero); an increase in the largest exponent is accompanied by a decrease

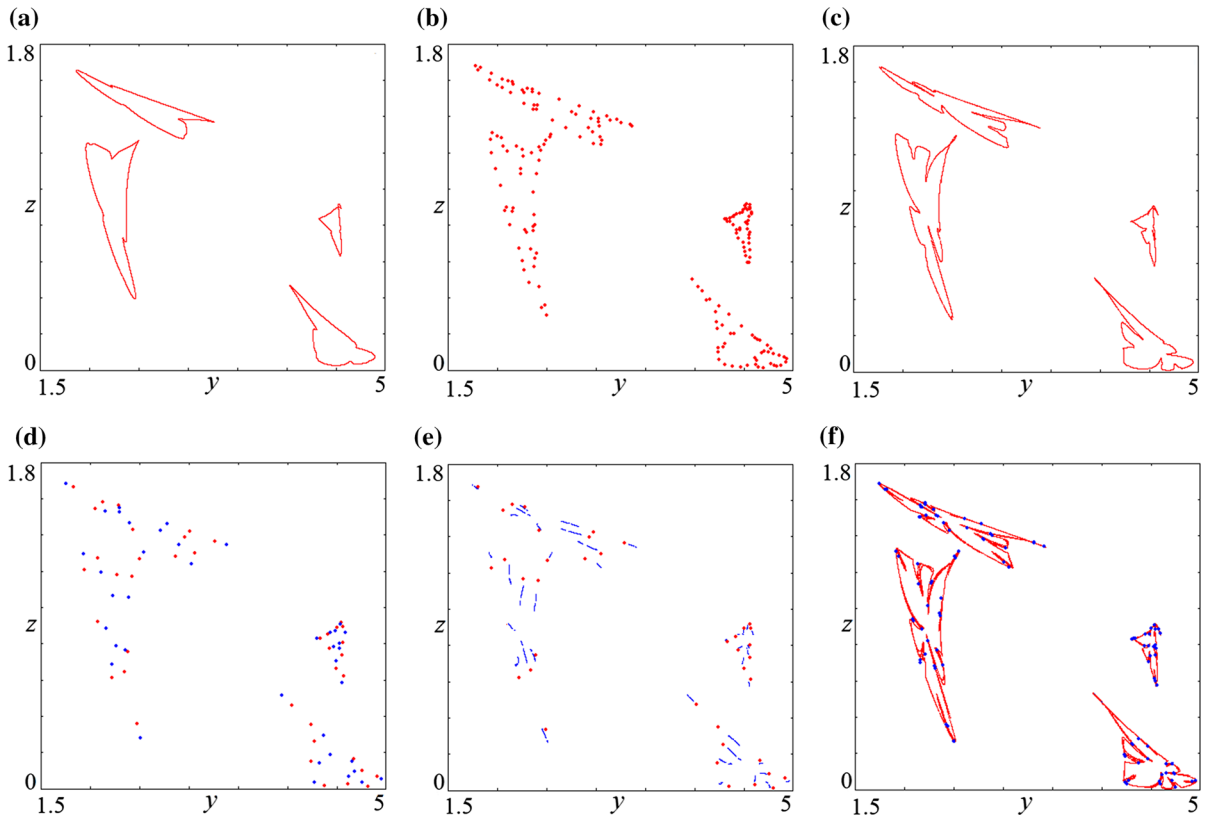

Fig. 9 Two-dimensional projections of phase portraits in the Poincaré section by surface $x = 0$ demonstrating formation of chaos via loss of smoothness of invariant curve, $g = 0.248$; **a** $m = 0.119$, T4:P4:T1:P1; **b** $m = 0.1195$, P47:T4:P4:T1:P1; **c** $m = 0.11955$, T4:P4:T1:P1; **d** $m = 0.119623$, P10:T4:P4:T1:P1 (red), P10:T4:P4:T1:P1 (blue); **e** $m = 0.119645$, P10:T4:P4:T1:P1 (red), chaos (blue); **f** $m = 0.119664$, chaos (red), P40:T4:P4:T1:P1 (blue). (Color figure online)

in the third. This picture is wellseen for chaos with one positive Lyapunov exponent (Fig. 8a). However, after the periodicity window at $m \approx 0.121456$, the dynamics of the third Lyapunov exponent changes; it begins to increase with the first. It can be assumed that for large values of the parameter m, the regime could become hyperchaotic. But due to the limited dynamical regime of the model (1) in the parameter space for this parameter, we observe that the trajectories begin to go to infinity before the third indicator reaches zero.

5 Conclusions

In the present work, on the example of the simplest model with hyperchaos, it is shown that the occurrence of hyperchaos may be associated with secondary Neimark–Sacker bifurcation and torus destruction.

It is well-known that Neimark–Sacker bifurcation corresponds to displacement of two multipliers at once beyond the unit circle of the plane of imaginary and real parts of the multipliers. This gives the prerequisites for emergence of two unstable directions. Torus destruction is usually associated with loss of smoothness of an invariant curve, or homoclinic bifurcation, or it can happen via Afraimovich–Shilnikov scenario, or another one [25]. Thus, on the threshold of bifurcation, various complex regimes can be observed: high-order synchronization tongues with period-doubling bifurcations inside them or multistability. In this regard, the presence of Neimark–Sacker bifurcation does not give an unambiguous opportunity for immediate occurrence of hyperchaos. However, a hyperchaotic set is formed

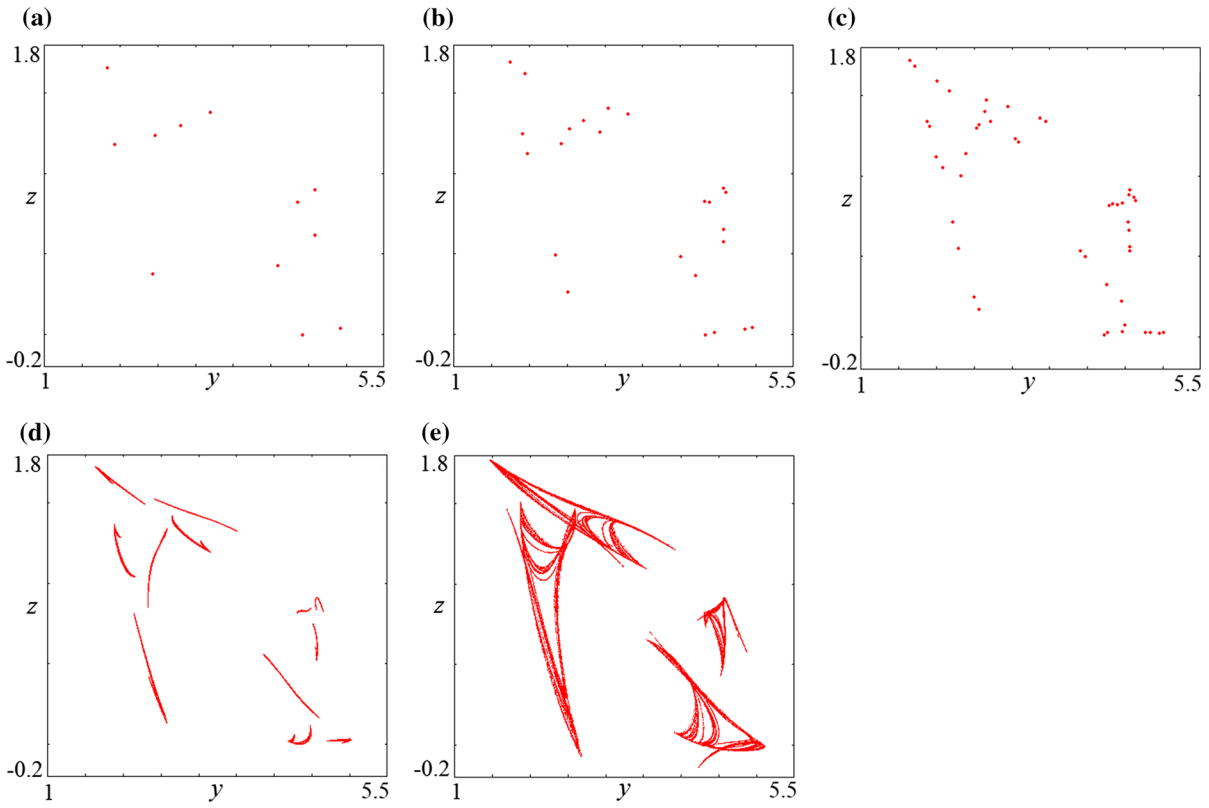

Fig. 10 Two-dimensional projections of phase portraits in the Poincaré section by surface $x = 0$ demonstrating formation of chaos via cascade of period-doubling bifurcations of the limit cycle of period-12, $g = 0.248$; **a** $m = 0.1207$, P3:T4:P4:T1:P1; **b** $m = 0.12075$, P6:T4:P4:T1:P1; **c** $m = 0.12083$, P12:T4:P4:T1:P1; **d** $m = 0.12085$, chaos; **e** $m = 0.121$, chaos

Table 5 Signature of the spectrum of the Lyapunov exponents for chaotic attractors occurring via cascade of period-doubling bifurcations of the limit cycle of period-12, $g = 0.248$

m	Regime	Λ_1	Λ_2	Λ_3	Λ_4
0.12085	C	0.0023	0.0000	−0.0059	−0.0878
0.121	C	0.0064	0.0000	−0.0117	−0.0839

and chaotic regimes occurring as a result of other different scenarios developed to this set.

The proposed scenario is sufficiently general and universal for dynamical systems of any higher dimension of their phase space. Wherein, for the systems with a large dimension of the phase space, the spectrum of Lyapunov exponents can contain more than two positive Lyapunov exponents, among others, in [8,9,32]. In ensembles of coupled oscillators with a number of subsystems exceeding two, the high-dimension hyperchaos is associated with dynamics of subsystems or destruction of tori of higher dimensions. As a result of torus destruction via secondary Neimark–Sacker bifurcation, it is possible to obtain hyperchaos with just two positive Lyapunov exponents, because they relate to two unstable directions occurring via such kind of bifurcation.

Acknowledgements Authors thank Igor Sataev, Alexey Kazakov and Serhiy Yanchuk for fruitful discussion of this problem.

Funding The work was carried out with the financial support of the Russian Foundation of Basic Research, Grant No. 18-32-00285 (Introduction, Sects. 2, 3, 4.1) and Russian Science Foundation, Grant No. 17-12-01008 (Sect. 4.2). Analysis of multistability was carried out in the frame of project of the Russian Foundation of Basic Research, Grant No. 19-02-00610.

Compliance with ethical standards

Conflict of interest The authors declare that they have no conflict of interest.

References

1. Schuster, H.G.: Deterministic chaos: an introduction, p. 220. Physik-Verlag, Weinheim (1984)
2. Mosekilde, E., Maistrenko, Y., Postnov, D.: Chaotic Synchronization: Applications to Living Systems, vol. 42. World Scientific, Singapore (2002)
3. Strogatz, S.H.: Nonlinear Dynamics and Chaos: With Applications to Physics, Biology, Chemistry, and Engineering. Westview Press, Boulder (2014)
4. Benettin, G., Galgani, L., Giorgilli, A., Strelcyn, J.-M.: Lyapunov characteristic exponents for smooth dynamical systems and for Hamiltonian systems: a method for computing all of them. Meccanica **15**, 9–30 (1980)
5. Pikovsky, A., Politi, A.: Lyapunov Exponents: A Tool to Explore Complex Dynamics. Cambridge University Press, Cambridge (2016)
6. Rossler, O.E.: An equation for hyperchaos. Phys. Lett. A **71**, 155–157 (1979)
7. Tamasevicius, A., Namajunas, A., Cenys, A.: Simple 4D chaotic oscillator. Electron. Lett. **32**, 957–958 (1996)
8. Blokhina, E.V., Kuznetsov, S.P., Rozhnev, A.G.: High-dimensional chaos in a gyrotron. IEEE Trans. Electron Dev. **54**, 188–193 (2007)
9. Rozental', R.M., Isaeva, O.B., Ginzburg, N.S., Zotova, I.V., Sergeev, A.S., Rozhnev, A.G.: Characteristics of chaotic regimes in a space-distributed gyroklystron model with delayed feedback. Russ. J. Nonlinear Dyn. **14**, 155–168 (2018)
10. Chen, Z., Yang, Y., Qi, G., Yuan, Z.: A novel hyperchaos system only with one equilibrium. Phys. Lett. A **360**, 696–701 (2007)
11. Wu, W., Chen, Z., Yuan, Z.: The evolution of a novel fourdimensional autonomous system: among 3-torus, limit cycle, 2-torus, chaos and hyperchaos. Chaos Solitons Fractals **39**, 2340–2356 (2009)
12. Li, Q., Tang, S., Zeng, H., Zhou, T.: On hyperchaos in a small memristive neural network. Nonlinear Dyn. **78**, 1087–1099 (2014)
13. Li, Q., Zeng, H., Li, J.: Hyperchaos in a 4D memristive circuit with infinitely many stable equilibria. Nonlinear Dyn. **79**, 2295–2308 (2015)
14. Biswas, D., Banerjee, T.: A simple chaotic and hyperchaotic time-delay system: design and electronic circuit implementation. Nonlinear Dyn. **83**, 2331–2347 (2016)
15. Fonzin, T.F., Kengne, J., Pelap, F.B.: Dynamical analysis and multistability in autonomous hyperchaotic oscillator with experimental verification. Nonlinear Dyn. **93**, 653–669 (2018)
16. Kapitaniak, T., Thylwe, K.E., Cohen, I., Wojewoda, J.: Chaos-hyperchaos transition. Chaos Solitons Fractals **5**, 2003–2011 (1995)
17. Harrison, M.A., Lai, Y.C.: Route to high-dimensional chaos. Phys. Rev. E **59**, R3799 (1999)
18. Kapitaniak, T., Maistrenko, Y., Popovych, S.: Chaos–hyperchaos transition. Phys. Rev. E **62**, 1972 (2000)
19. Yanchuk, S., Kapitaniak, T.: Symmetry-increasing bifurcation as a predictor of a chaos–hyperchaos transition in coupled systems. Phys. Rev. E **64**, 056235 (2001)
20. Nikolov, S., Clodong, S.: Hyperchaos–chaos–hyperchaos transition in modified Rössler systems. Chaos Solitons Fractals **28**, 252–263 (2006)
21. Harikrishnan, K.P., Misra, R., Ambika, G.: On the transition to hyperchaos and the structure of hyperchaotic attractors. Eur. Phys. J. B **86**, 1–12 (2013)
22. Li, Q., Tang, S., Yang, X.S.: Hyperchaotic set in continuous chaos–hyperchaos transition. Commun. Nonlinear Sci. Numer. Simul. **19**, 3718–3734 (2014)
23. Munteanu, L., Brian, C., Chiroiu, V., Dumitriu, D., Ioan, R.: Chaos–hyperchaos transition in a class of models governed by Sommerfeld effect. Nonlinear Dyn. **78**, 1877–1889 (2014)
24. Gonchenko, S.V., Ovsyannikov, I.I., Simò, C., Turaev, D.: Three-dimensional Hénon-like maps and wild Lorenz-like attractors. Int. J. Bifurc. Chaos **15**, 3493–3508 (2005)
25. Gonchenko, A.S., Gonchenko, S.V., Shilnikov, L.P.: Towards scenarios of chaos appearance in three-dimensional maps. Russ. J. Nonlinear Dyn. **8**, 3–28 (2012). (Russian)
26. Gonchenko, A., Gonchenko, S., Kazakov, A., Turaev, D.: Simple scenarios of onset of chaos in three-dimensional maps. Int. J. Bifurc. Chaos **24**, 1440005 (2014)
27. Stankevich, N.V., Dvorak, A., Astakhov, V., Jaros, P., Kapitaniak, M., Perlikowski, P., Kapitaniak, T.: Chaos and hyperchaos in coupled antiphase driven toda oscillators. Regul. Chaotic Dyn. **23**, 120–126 (2018)
28. Kuznetsov, A.P., Sedova, Y.V.: Coupled systems with hyperchaos and quasiperiodicity. J. Appl. Nonlinear Dyn. **5**, 161–167 (2016)
29. Rech, P.C.: Hyperchaos and quasiperiodicity from a four-dimensional system based on the Lorenz system. Eur. Phys. J. B **90**, 251 (2017)
30. Amabili, M., Karagiozis, K., Païdoussis, M.P.: Hyperchaotic behaviour of shells subjected to flow and external force. In: ASME 2010 3rd Joint US-European Fluids Engineering Summer Meeting collocated with 8th International Conference on Nanochannels, Microchannels, and Minichannels, American Society of Mechanical Engineers, pp. 1209–1217 (2010)
31. Kuznetsov, A.P., Migunova, N.A., Sataev, I.R., Sedova, YuV, Turukina, L.V.: From chaos to quasi-periodicity. Regul. Chaotic Dyn. **20**, 189–204 (2015)
32. Stankevich, N.V., Astakhov, O.V., Kuznetsov, A.P., Seleznev, E.P.: Exciting chaotic and quasi-periodic oscillations in a multicircuit oscillator with a common control scheme. Tech. Phys. Lett. **44**, 428–431 (2018)
33. Anishchenko, V.S., Nikolaev, S.M.: Generator of quasiperiodic oscillations featuring two-dimensional torus doubling bifurcations. Tech. Phys. Lett. **31**, 853–855 (2005)
34. Anishchenko, V.S., Nikolaev, S.M., Kurths, J.: Peculiarities of synchronization of a resonant limit cycle on a two-dimensional torus. Phys. Rev. E **76**, 046216 (2007)
35. Kuznetsov, A.P., Stankevich, N.V.: Autonomous systems with quasiperiodic dynamics. Examples and their properties: review. Izv. VUZ Appl. Nonlinear Dyn. **23**, 71–93 (2015). (in Russia)
36. Kuznetsov, N.V.: The Lyapunov dimension and its estimation via the Leonov method. Phys. Lett. A **380**, 2142–2149 (2016)
37. Kuznetsov, N.V., Leonov, G.A., Mokaev, T.N., Prasad, A., Shrimali, M.D.: Finite-time Lyapunov dimension and hid-

den attractor of the Rabinovich system. Nonlinear Dyn. **92**, 267–285 (2018)
38. Zhusubaliyev, Z.T., Mosekilde, E.: Formation and destruction of multilayered tori in coupled map systems. Chaos **18**, 037124 (2008)
39. Zhusubaliyev, Z.T., Laugesen, J.L., Mosekilde, E.: From multi-layered resonance tori to period-doubled ergodic tori. Phys. Lett. A **374**, 2534–2538 (2010)
40. Vitolo, R., Broer, H., Simó, C.: Routes to chaos in the Hopf-saddle-node bifurcation for fixed points of 3D-diffeomorphisms. Nonlinearity **23**, 1919–1947 (2010)
41. Broer, H., Simó, C., Vitolo, R.: Quasi-periodic bifurcations of invariant circles in low-dimensional dissipative dynamical systems. Regul. Chaotic Dyn. **16**, 154–184(2011)
42. Komuro, M., Kamiyama, K., Endo, T., Aihara, K.: Quasi-periodic bifurcations of higher-dimensional tori. Int. J. Bifurc. Chaos **26**, 1630016 (2016)
43. Wieczorek, S., Krauskopf, B., Lenstra, D.: Mechanisms for multistability in a semiconductor laser with optical injection. Opt. Commun. **183**, 215–226 (2000)
44. Stankevich, N.V., Volkov, E.I.: Multistability in a three-dimensional oscillator: tori, resonant cycles and chaos. Nonlinear Dyn. **94**, 2455–2467 (2018)